Nanoscale

Accepted Manuscript

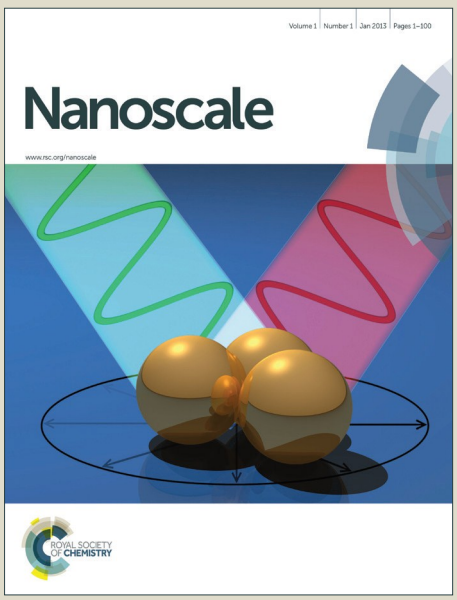

This is an *Accepted Manuscript*, which has been through the Royal Society of Chemistry peer review process and has been accepted for publication.

Accepted Manuscripts are published online shortly after acceptance, before technical editing, formatting and proof reading. Using this free service, authors can make their results available to the community, in citable form, before we publish the edited article. We will replace this *Accepted Manuscript* with the edited and formatted *Advance Article* as soon as it is available.

You can find more information about *Accepted Manuscripts* in the Information for Authors.

Please note that technical editing may introduce minor changes to the text and/or graphics, which may alter content. The journal's standard Terms & Conditions and the Ethical guidelines still apply. In no event shall the Royal Society of Chemistry be held responsible for any errors or omissions in this *Accepted Manuscript* or any consequences arising from the use of any information it contains.

ROYAL SOCIETY OF CHEMISTRY

www.rsc.org/nanoscale

Moderate temperature processed solar cell with record-high-Voc of 1.61 V and FF of 0.77 based on solvent annealed $CH_3NH_3PbBr_3$/ICBA active layer

Chun-Guey Wu[a,b,*], Chien-Hung Chiang[b], Sheng Hsiung Chang[b]

[a]*Department of Chemistry and* [b]*Research Center for New Generation Photovoltaics, National Central University, Jhong-Li, 32001, Taiwan, ROC.*

E-mail address of Professor C. G. Wu: t610002@cc.ncu.edu.tw

Graphical abstract

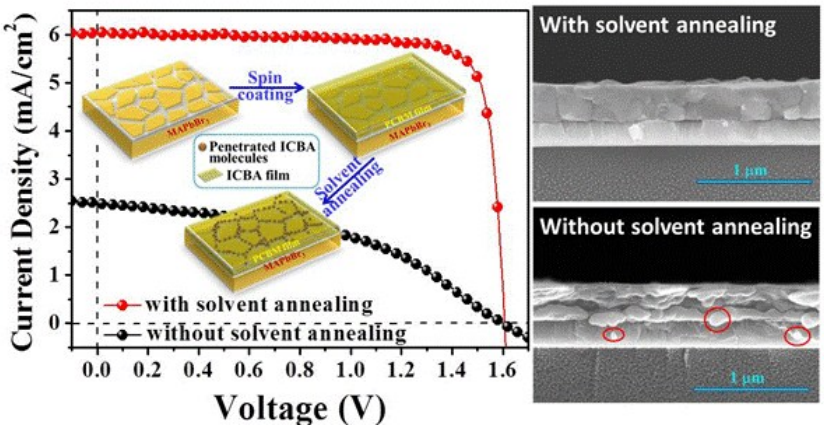

The inverted perovskite solar cell with record-high Voc of 1.61 V based on $CH_3NH_3PbBr_3$ film fabricated at ambient atmosphere and moderate temperature (~ 100 ^oC) was reported. ICBA with high LUMO level was used as an acceptor to realize high Voc and as a mend agent to increase the efficiency by penetrating into the defects/voids of $CH_3NH_3PbBr_3$ film to form pseudo bulk heterojunction structure. Solvent annealing of the donor/acceptor layer was shown to be a very simple and effective device engineering to improve the performance of the cell with low quality $CH_3NH_3PbBr_3$ film.

Nanoscale Accepted Manuscript

Abstract:

High open-circuit voltage inverted perovskite solar cell based on $CH_3NH_3PbBr_3$ absorber and ICBA acceptor is reported. $CH_3NH_3PbBr_3$ film fabricated under the ambient atmosphere at low temperature (~ 100^oC) using two-step spin-coating method composed of aggregated nano-grains. Upon solvent annealing of $CH_3NH_3PbBr_3$ /ICBA film, the efficiency of resulting cell increases from 1.71% to 7.50% with the remarkably high open circuit voltage (V_{oc}) of *ca.* 1.60 V. ICBA acts not only as high LUMO acceptor to realize high Voc but also as a mend agent to increase the efficiency of the cell by penetrating into the defects/voids of $CH_3NH_3PbBr_3$ film *via* solvent annealing as evidenced by TRPL, XPS and SEM data. Solvent annealing of the active layer was proved to be a simple and effective device engineering to improve the efficiency of perovskite cell based on low quality film and the Voc of the inverted perovskite cell can be tuned by the LUMO level of the acceptor was revealed. $CH_3NH_3PbBr_3$/ICBA film is semi-transparent with an average 50% transmittance in the visible light. Low-temperature processed $CH_3NH_3PbBr_3$ solar cell with high Voc and semi-transparent absorber has great potential for applying as the top cell in a tandem solar cell.

Nanoscale Accepted Manuscript

1. Introduction

Organic-inorganic lead halide perovskite has attracted immense attention over the last several years due to perovskite based solar cells have shown great promise for achieving high-efficiency and low-cost.[1-13] Device based on $CH_3NH_3PbBr_3$ with high LUMO (-3.4 eV) and deep HOMO (-5.6 eV) levels[14] can achieve high *Voc* and be semi-transparent. Therefore $CH_3NH_3PbBr_3$ based cell is a suitable candidate to be used as a top cell of all tandem solar cells. Qiu[15] *et al.* applied $CH_3NH_3PbBr_3$ in a regular mesoscopic (mp) TiO_2 solar cell, using poly[N-9-hepta-decanyl-2,7-carbazole-alt-3,6-bis-(thiophen-5-yl)-2,5-dioctyl-2,5-di-hydropyrrolo[3,4-]pyrrole-1,4-dione] (PCBTDPP) hole transport layer to achieve the *Voc* of 1.16 V with power conversion efficiency (PCE) of 3.04%. Instead of using mesoscopic TiO_2 anode, Edri[16] *et al.* used mesoporous alumina (on dense (d) TiO_2) anode and N,N'-dialkyl perylenediimide (PDI) hole transport material to enhance the V_{oc} to 1.3 V, however, the efficiency of the cell is only 0.56%. Seok[17] *et al.* reported the fabrication of the regular d-TiO_2/mp-TiO_2/ $MAPbBr_3$/PIF8-TAA cells and the highest V_{oc} and efficiency of the devices are 1.4 V and 6.7%, respectively. Very recently Heo[18] *et al.* used the similar regular cell architecture, fabrication procedure and components as those used by Seok[17] except adding HBr(aq) in $MAPbBr_3$ precursor solution. The resulting cell has the highest efficiency of 10.4% with very high *Voc* of 1.51 V.

Regular (DSC-type) perovskite solar cells based on $MAPbBr_3$ absorber have been proved to realize high V_{oc}.[15-19] However the architectures of the reported high *Voc* $CH_3NH_3PbBr_3$ cells are all using mesoscopic or dense planner TiO_2 film as an anode. Mesoporous or high quality dense TiO_2 film used in the high efficiency devices often requires high-temperature (above 450 ^oC) treatment. Such severe fabrication conditions could limit the future development of perovskite solar cells, particularly in the flexible or tandem cells. Furthermore, Snaith[20] *et al*. found that the light-induced

Nanoscale Accepted Manuscript

desorption of the surface-adsorbed oxygen could be the critical reason for the instability of the mesoporous TiO_2-based solar cells. On the other hand, the inverted cell (perovskite acts as an absorber and hole transporter) can be fabricated at low temperature and no metal oxide charge transporter is needed. Furthermore, the theoretical (maximum) *Voc* of the mesoscopic (or regular) solar cells is the energy difference between the Fermi level of the electron transporter and the HOMO of the donor.[21] Therefore, the theoretic V_{oc} for a mesoscopic (or regular) perovskite solar cell based on $CH_3NH_3PbBr_3$ (with a HOMO level at ~ -5.6 eV *vs*. vacuum) absorber and TiO_2 (quasi Fermi energy level ~ -4.0 eV *vs.* vacuum) electron transporter is 1.6 V. Whereas in an ideal case without any energy loss at all interfaces of the device, the theoretical Voc for the inverted $CH_3NH_3PbBr_3$ cell is close to the band gap of the absorber, *i.e.,* 2.2 eV. Even considering the Shockley–Queisser limit proposed by Shockley[22] *et al.*, V_{oc} higher than 1.6 V for a single p-i-n junction $CH_3NH_3PbBr_3$ solar cell is achievable. It provides a great possibility to fabricate solar cell with high open-circuit voltage. The inverted structure also has the advantages of simple structure and fabricating at low temperature, hence can be a good architecture for further technology development, such as roll-to-roll production or tandem cell. Furthermore, high quality absorber film is essential for achieving high efficiency of perovskite solar cell. Nevertheless, it may have some difficulties to fabricate high quality $CH_3NH_3PbBr_3$ film using a simple and reproducible method. In this study, we demonstrated a new method to improve the photovoltaic performance of the cell based on low quality $CH_3NH_3PbBr_3$ film simply by solvent annealing of the perovskite/acceptor layer.

2. Results and discussion

Preparation and properties of $CH_3NH_3PbBr_3$ film on PEDOT:PSS.

Nanoscale Accepted Manuscript

The process for fabricating the inverted $CH_3NH_3PbBr_3$ solar cell is illustrated in Figure 1 and the detailed preparation procedures and materials used can be found in the experimental section. The layout of the device is the general architecture of the inverted perovskite solar cell:[23] $CH_3NH_3PbBr_3$ acts as an absorber as well as hole transporter and fullerene derivative functions as an acceptor. Spin coating used for preparing perovskite films in this paper is a well-known technique to deposit thin film on a substrate. Both one-step and two-step methods were used in this study to prepare $CH_3NH_3PbBr_3$ and the SEM images of the resulting film are displayed in Figure 2. It was shown that only isolated grains were formed on PEDOT:PSS surface when one-step method is used, due to $CH_3NH_3PbBr_3$ crystallizes very fast. It seems that to prepare good quality $CH_3NH_3PbBr_3$ film with one-step method, more creative strategies need to be found. On the other hand two-step spin coating method can grow full-coverage $CH_3NH_3PbI_3$ film on PEDOT:PSS although it is not a very smooth film. In a two-step method, $PbBr_2$ has less ionic characteristic (compared to $CH_3NH_3PbBr_3$) therefore better quality film can be first spin-coated on the surface of PEDOT:PSS. $CH_3NH_3PbBr_3$ was then formed by intercalating MABr into $PbBr_2$ at the second step. The deposition and intercalation of $PbBr_2$ film is not sensitive to H_2O therefore the preparation of $CH_3NH_3PbBr_3$ film can be carried-out under ambient atmosphere at moderate temperature (~ 100 ^oC). However, two-step spin-coating method although can grow full-coverage $CH_3NH_3PbI_3$ film on PEDOT:PSS, the quality of the resulting film (displayed in middle of Figure 2) is still not good enough to achieve high photovoltaic performance. SEM images (displayed in the left side of Figure 2) show that $PbBr_2$ film deposited on PEDOT:PSS contains lots of holes. It could be one of the reasons that the quality of the corresponding $CH_3NH_3PbBr_3$ film is not so good. It seems that to fabricate high quality $CH_3NH_3PbBr_3$ film *via* two-step method for the inverted perovskite solar cell is not as easy as fabricating high quality $CH_3NH_3PbI_3$

Nanoscale Accepted Manuscript

film.[26]

To prepare highly pure, flat and full covered $CH_3NH_3PbBr_3$ film using two-step spin coating method, several parameters need to be concerned. Not only the concentration and amount of the two precursor solutions but also the design of spin coater and spin programs will affect the quality of the resulting film. For example for the same $PbBr_2$ film, the concentration and amount of MABr/IPA solution will affect the reaction time (the reaction time is the time required to evaporate all the solvent molecules of the solution under very fast spin) and therefore the morphology and stoichiometry of the resulting perovskite film. Lots of parameters were tried in this study and the parameters to prepare the best quality $CH_3NH_3PbBr_3$ film are: 50 μl, 0.5 M $PbBr_2$/DMF precursor solution under the spin of 2000 rpm for 30 sec and 30 μl, 15 mg/mL MABr/IPA under a spin rate of 2000 rpm for 30 sec in a 1.5 cm x 1.5 cm PEDOT:PSS coated ITO substrate. To avoid the interminable description on the experimental results, for each experimental condition, only the cells with the highest efficiency were shown in the paper. Nevertheless, to demonstrate the process on searching for the best quality $CH_3NH_3PbBr_3$ film, the effects of MABr/IPA concentration on the properties of the resulting $CH_3NH_3PbBr_3$ film and the photovoltaic performance of the corresponding inverted cell are discussed.

The phase, crystallinity, purity and surface morphology of $CH_3NH_3PbBr_3$ films prepared using various concentrations of MABr/IPA solutions were investigated with X-ray diffraction, EDS analysis and SEM imaging. The XRD patterns of the films are illustrated in Figure 3 and the original 2D diffraction data are displayed in Figure S1 of the Electronic Supporting Information (ESI). Pure $CH_3NH_3PbBr_3$ phase (showed only six sharp diffraction peaks appeared at 2θ of 14.57°, 20.83°, 29.80°, 33.35°, 37.9°, 42.78°, and 45.56°, corresponding to (1 0 1), (1 2 1), (0 4 0), (1 4 1), (2 4 2), and (0 6 0) planes respectively[16,24]) can be obtained by using proper concentration of

Nanoscale Accepted Manuscript

MABr/IPA solution in the second step. When insufficient MABr/IPA was used, some unreacted $PbBr_2$ phase was detected in GIXRD (Grazing Incidence X-Ray Diffraction) pattern. When the concentration of MABr/IPA is too high, although no additional diffraction peak was found, extra MABr or its decomposed bromide will exist as an impurity in the film, as revealed with SEM-EDS data: The Br/Pb ratio of the resulting film is higher than 3 when 20 mg MABr/mL IPA was used. On the other hand, the Pb:Br atomic ratio for the pure phase films (prepared from 15 mg MABr/mL IPA solution) is 1:3 and no other halide was detected (the original EDS data are displayed in Figure S2, ESI). XRD and EDS data suggest that highly pure $CH_3NH_3PbBr_3$ film can be made by using proper fabrication condition in a two-step method. Furthermore the SEM images (illustrated in Figure S3, ESI) of pure $CH_3NH_3PbBr_3$ film is full covered, nevertheless films with unreacted $PbBr_2$ or with extra bromides all have poorer morphology containing more defects/holes.

The photovoltaic performance of the inverted cell based on $CH_3NH_3PbBr_3$ and the device engineering to improve the cell performance.

PCBM ([6,6]-phenyl-C61-butyric acid methyl ester) having high electron mobility[25] and suitable band structure was generally used as an acceptor in organic photovoltaics and inverted perovskite solar cells. The LUMO level of PCBM is compatible with that of $CH_3NH_3PbBr_3$ (which has LUMO level 0.5 eV higher than that for PCBM, see Figure 4) for efficient electron injection. As expect the device based on $CH_3NH_3PbBr_3$ donor and PCBM acceptor exhibits the V_{oc} of 1.38 V (see Table 1) which is higher than that of the inverted $CH_3NH_3PbI_3$ solar cells using the same acceptor.[6,23,29,30] However the power conversion efficiency (PCE) is very low (less than 1%) with very small Jsc and FF. Low FF value is probably because of $CH_3NH_3PbBr_3$ film is formed by the aggregated nano-grains not a smooth, continuous

Nanoscale Accepted Manuscript

film as the SEM images shown in Figure 2. The film containing a lot of small holes and grain boundaries has high inter-particle resistance. The low Jsc is due to not only the poor quality of the film but also the large band gap of $CH_3NH_3PbBr_3$ which cannot absorb the sun light efficiently. If the quality of $CH_3NH_3PbBr_3$ film is hard to improve further, device engineering could be an alternative way to improve the photovoltaic performance of the inverted $CH_3NH_3PbBr_3$ cell.

If the holes and grain boundaries of $CH_3NH_3PbBr_3$ film is the reason for the poor photovoltaic performance. It may be mended by filling the voids with acceptor. When the active $CH_3NH_3PbBr_3$/PCBM film was solvent annealed (the detail description of the solvent annealing was described in the experimental section) for 24 hours before depositing Ca/Al electrode, the PCE of the resulting cell increases form 0.86% to 5.6% with significant enhance in both Jsc and FF values. Solvent annealing of the active film may allow PCBM molecules penetrate slowly into the inside (not just the surface) holes or grain boundaries of $CH_3NH_3PbBr_3$ film to mend the defects by forming pseudo bulk-heterojunction structure, therefore improve the performance of the cell. The function of the solvent annealing will be discussed more in detail in the later paragraphs. Even with solvent annealing of the active layer, the efficiency of the device is also sensitive to the purity of $CH_3NH_3PbBr_3$ film. As the photovoltaic data listed in Table 1, cells based on $CH_3NH_3PbBr_3$ containing unreacted $PbBr_2$ (prepared with low MABr/IPA concentration) or extra bromides (prepared with high MABr/IPA concentration) all result in low efficiency of the corresponding cell (the I-V curves of the cell based on $CH_3NH_3PbBr_3$ prepared from three different MABr/IPA concentrations were displayed in Figure S4, ESI).

As the frontier orbital energy level illustrated in Figure 4 and the good photovoltaic performance of the inverted ITO/PEDOT:PSS/$CH_3NH_3PbI_3$/PCBM/Ca/Al cell[26] suggest that large driving force is not necessary for injecting the excited

Nanoscale Accepted Manuscript

electron from perovskite absorber to PCBM acceptor since the LUMO levels for $MAPbI_3$ and PCBM are very close. Data in Figure 4 also show that the LUMO level[17] of $CH_3NH_3PbBr_3$ is *ca.* 0.5 V higher than that of $CH_3NH_3PbI_3$. Therefore acceptor with the LUMO level higher (up to 0.5 eV) than PCBM could be applied in $CH_3NH_3PbBr_3$ based device to increase the V_{oc} of the cell. ICBA (1′,1″,4′,4″-Tetrahydro-di[1,4]metha-nonaphthaleno[1,2:2′,3′,56,60:2″,3″][5,6] fullerene-C_{60})**,** another derivative of the fullerene family[31] commonly used in OPV, with LUMO level *ca.* 0.2 eV higher than that of PCBM was chosen as an example to demonstrate the concept. The photovoltaic parameters of the inverted $CH_3NH_3PbBr_3$ cell based on ICBA acceptor with and without solvent annealing of the active layer are also listed in Table 1. Without solvent annealing, the photovoltaic parameters of the cell using ICBA as an electron transporter are all larger than those for the device using PCBM acceptor. It is due to that the viscosity of ICBA/chlorobenzene (CB) solution is lower than that of PCBM/CB solution. Therefore during spin coating process, more ICBA (compared to PCBM) molecules diffuse into the inside voids of $CH_3NH_3PbBr_3$ film. Remarkably, the device achieves a Voc of 1.60 V which is the highest V_{oc} for all single junction solar cell reported in the newest Solar Cell Efficiency Tables (version 46).[32] Upon solvent annealing of the active layer, the efficiency of the cell increases from 1.71% to 7.5% with significant enhance in both Jsc and FF values but keeps the same Voc, just like the cell based on PCBM acceptor. Interestingly, the Voc enhancement (0.22 = 1.60-1.38 (V)) of using ICBA to replace PCBM as an acceptor is close to the difference (0.2 V) of the LUMO energy levels between PCBM and ICBA. The results further supported that the driving force needed for the efficient charge separation between $CH_3NH_3PbBr_3$ and acceptor could be very small. In this sense, ICBA may not be the best acceptor (or the optimal acceptor) for the inverted $CH_3NH_3PbBr_3$ solar cell to achieve the high Voc. An inverted

Nanoscale Accepted Manuscript

$CH_3NH_3PbBr_3$ solar cell with Voc higher than 1.6 V is possible if a highly conducting acceptor with the LUMO level higher than ICBA can be found. The IPCE curve of the champion inverted $CH_3NH_3PbBr_3$ cell is shown in Figure 5 (a). The curve shows a strong spectral response at the wavelength from 375 nm to 525 nm (with the highest efficiency close to 70% at 375 nm) and then drops quickly to zero at the wavelength of 550 nm, consisting with the absorption profile of $CH_3NH_3PbBr_3$ film (illustrated in Figure 5 (b)) and the semi-transparent yellow-colored ITO/PEDOT:PSS/ $CH_3NH_3PbBr_3$ film (revealed in Figure S5, ESI). Compared to the absorption spectrum of $CH_3NH_3PbBr_3$ single crystal,[33] the slope of the Urbach tail of our sample is smaller, indicating smaller crystalline domain size.

The Voc is quite reproducible for the inverted $CH_3NH_3PbBr_3$ cell using ICBA as an acceptor. The Voc statistics based on 29 cells (displayed in Figure S6, ESI) clearly showed that high Voc is a general property for the inverted cell based on $CH_3NH_3PbBr_3$ donor and ICBA acceptor. Moreover, the photographs displayed in Figure S5, ESI also reveal that $CH_3NH_3PbBr_3$/ICBA film is more transparent compared to $CH_3NH_3PbBr_3$/PCBM and its transparency is similar to that of $CH_3NH_3PbBr_3$ film due to the low absorption characteristic of ICBA. Weak absorption in the visible light is another advantage of ICBA acceptor, since in a perovskite solar cell, perovskite film plays a key role in the light absorption and hole transporting, while the acceptor functions mainly as an electron transporter without contributing to the short circuit current (Jsc) of the cell. ICBA with low absorption and high LUMO level can enhance the Voc of the inverted $CH_3NH_3PbBr_3$/ICBA cell and keep still the translucent nature of $CH_3NH_3PbBr_3$ film. Semi-transparent photovoltaic device with high Voc has great potential for applying as the top cell in a tandem solar cell.

The function of the solvent annealing of the active layer: mending the defects

Nanoscale Accepted Manuscript

of $CH_3NH_3PbBr_3$ film and forming a pseudo-heterojunction structure by penetrating the acceptor into perovskite film.

High quality absorber is essential for achieving high efficiency of perovskite solar cell. $CH_3NH_3PbBr_3$ is an ionic coordination solid state material, the vacancy or grain boundary of the film can be regarded as the defect sites which may hinder the carrier transport or quench the carriers and excirons.[34] Snaith *et al.* had used organic iodide[35] or pyridine[36] to passivate perovskite film to improve the photovoltaic performance of the cell. Zhang *et al.* used organic silane[37] as a passivation agent for perovskite film and showed the improvement in efficiency and water resistance of the device. In the previous paragraphs we had shown that the inverted cell based on aggregated $CH_3NH_3PbBr_3$ nano-grains has very low efficiency. However, when the active (donor/acceptor) layer was solvent annealed for 24 hours at room temperature, the performance of the cells enhances tremendously, especially in Jsc and FF. We have proposed that the enhancement in the photovoltaic performance is due to some acceptor molecules penetrate into the holes/grain boundaries of $CH_3NH_3PbBr_3$ film to form pseudo bulk-heterojunction structure as illustrated in Figure 6. It can also be regarded as the defects of $CH_3NH_3PbBr_3$ film were mended by the acceptor molecules. The merit of using acceptor as a mending/passivating agent is no extra layer of organic compound is used. Organic compound generally has low conductivity, extra layer of organic compound may increase the series resistance of the cell, decreases the efficiency. No extra passivation agent used also simplifies the fabrication procedure, reduces the cost of the cell.

In order to get the evidences regarding to the penetration of the acceptor, PL spectra of PEDOT:PSS/$CH_3NH_3PbBr_3$ and PEDOT:PSS/$CH_3NH_3PbBr_3$/ICBA with or without solvent annealing were taken and presented in Figure 7. As expected, the PL intensity (Figure 7 (a)) of $CH_3NH_3PbBr_3$ film decreases by adding PCBM or ICBA.

Nanoscale Accepted Manuscript

Nevertheless without solvent annealing only 50% and 60% of PL was quenched by PCBM and ICBA, respectively. When the donor/acceptor layer was solvent annealed for 24 hours, 88% and 93% of PL was quenched by PCBM and ICBA, respectively. To further address the exciton dynamics at the interface between the $CH_3NH_3PbBr_3$ and the acceptor (ICBA), time-resolved photoluminescence (TR-PL) spectra of glass/$CH_3NH_3PbBr_3$, glass/$CH_3NH_3PbBr_3$/ICBA with and without solvent annealing were taken and presented in Figure 7 (b). The PL quenching after solvent annealing (see Figure 7 (a)) indicates that the excitons were efficiently dissociated at the interface between the $CH_3NH_3PbBr_3$ and the ICBA when the solvent annealing process was used to improve the contact interface between the $CH_3NH_3PbBr_3$ and ICBA. TR-PL reflects the exciton dynamics in $CH_3NH_3PbBr_3$ film. Two type of quenching processes: the non-radiative lifetime (τ_{NR}) and radiative lifetime (τ_R) of excitons in $CH_3NH_3PbBr_3$ film can be resolved by fitting the normalized time-dependent photoluminescence using a 2-constant exponential decay function as follows[38] and the fitting results were listed in Table S1, ESI.

$$I_{PL} = A_{NR}\exp(-t/\tau_{NR}) + A_R\exp(-t/\tau_R)$$

where A_{NR} is the normalized amplitude of non-radiative exciton annihilation, A_R is the normalized amplitude of radiative excitons, τ_{NR} is the lifetime for the non-radiative exciton annihilation, and τ_R is the radiative exciton lifetime. The black curve in the Figure 7 (b) shows the average excitonic dynamics of $CH_3NH_3PbBr_3$ film (bulk and top surface). The residual exciton dynamics (red curve in the Figure 7 (b)) indicates that the charge transfer radius (depletion region)[39] at the interface between $CH_3NH_3PbBr_3$ and ICBA is shorter than the thickness of $CH_3NH_3PbBr_3$ film. The radiative exciton lifetime (non-radiative exciton lifetime) is extended from 4.66 ns (2.05 ns) to 8.83 ns (2.73 ns) when ICBA was added on the top of $CH_3NH_3PbBr_3$

Nanoscale Accepted Manuscript

without solvent annealing. It suggests that the defects on the top surface of $CH_3NH_3PbBr_3$ film are reduced by contacting ICBA. When the solvent annealing process is performed, the exciton lifetime decreased from 8.83 ns to 1.32 ns, which originates from the accelerated exciton dissociation[40] at the interface between $CH_3NH_3PbBr_3$ and ICBA. It means that the contact interface between $CH_3NH_3PbBr_3$ and ICBA was improved by the solvent annealing process. In other words, the ICBA penetrates into the interstices of the $CH_3NH_3PbBr_3$ thin film to form a pseudo bulk-heterojunction $CH_3NH_3PbBr_3$/ICBA film. Long term solvent annealing at low temperature does allow acceptor molecules to penetrate gradually into the vacancies and grain boundaries of $CH_3NH_3PbBr_3$ film to mend the defects of the film to improve the Jsc and FF of the cell.

Another evidence for the penetration of ICBA into $CH_3NH_3PbBr_3$ film was from the cross section SEM images of ITO/PEDOT:PSS/$CH_3NH_3PbBr_3$/ICBA films with and without solvent annealing as displayed in Figure 8. The thickness of $CH_3NH_3PbBr_3$ films estimated from the image is *ca.* 400 nm which is close to that measured with the surface profile meter. ITO/PEDOT:PSS/ $CH_3NH_3PbBr_3$/ICBA film without solvent annealing is very fragile, it falls apart (some small orifices were marked with the red circle in the image) when broke in-half for cross section viewing. On the other hand, the film is robust after solvent annealing: it keeps intact when broken in-half. The SEM data supported that some holes in $CH_3NH_3PbBr_3$ film were filled with ICBA *via* long-time solvent annealing. Unfortunately the resolution of the SEM-EDS is not high enough to distinguished ICBA from $CH_3NH_3PbBr_3$ and the film is so flat that the distribution of ICBA in $CH_3NH_3PbBr_3$/ICBA cannot be revealed. Nevertheless solvent annealing of pure $CH_3NH_3PbBr_3$ film by chlorobenzene did not change the crystalline domain size and crystallinity of $CH_3NH_3PbBr_3$ film as probed with XRD. Therefore the efficiency of the corresponding inverted cell is within

Nanoscale Accepted Manuscript

the experimental uncertainty. The significant improvement in efficiency upon solvent annealing is not due to the change of $CH_3NH_3PbBr_3$ film.

To get the direct evidence for the penetration of acceptor molecules, XPS depth profile analysis was performed on $CH_3NH_3PbBr_3$/PCBM film (PCBM containing O atoms which $CH_3NH_3PbBr_3$ did not have) with and without solvent annealing. Four elements (Pb, Br, C and O) were probed and the distribution of O atom was extracted from the results and displayed in Figure 9 (the distributions of all 4 elements in two samples are illustrated in Figure S7, ESI). On the surface of the active film, the oxygen content of annealed sample is smaller than that for the non-annealed one since some PCBM molecules already permeated inside $CH_3NH_3PbBr_3$ film. Starting from the second layer the solvent annealed film has larger oxygen content compared to the film without solvent annealing. Depth profile XPS data provide a direct evidence that more acceptor molecules penetrate inside $CH_3NH_3PbBr_3$ film upon solvent annealing of the active layer..

Current hysteresis and long-term stability of the inverted $CH_3NH_3PbBr_3$ solar cell.

Photocurrent hysteresis at various photovoltaic measuring conditions has been observed in some perovskite solar cells. It is an indication of poor quality/structure defects of perovskite absorber, poor device interphase and the un-balance between the hole and electron transporting in the device.[41,42] The efficiency for a cell with hysteresis may not truly represent the photovoltaic performance of the device. The I-V curves for our champion inverted $CH_3NH_3PbBr_3$ cell exhibits no current hysteresis at (two) scan directions but slightly hysteresis was observed at various scan rates although is very limit (see Figure S7, ESI). The photovoltaic performance of

Nanoscale Accepted Manuscript

the cells was improved by solvent annealing of the active film to form pseudo bulk-heterojunction structure. However, ICBA molecules may not be able to fill all holes/grain boundaries especially the side close to the substrate. In other words the defects of $CH_3NH_3PbBr_3$ film cannot be passivated entirely by solvent annealing. More creative synthetic strategy need to be developed to prepare better quality $CH_3NH_3PbBr_3$ film to increase the cell efficiency and reduce the current hysteresis totally. Furthermore, the inverted $CH_3NH_3PbBr_3$ solar cell is stable in inert atmosphere, without packing the device retains 90% of its initial efficiency after storing in a glove box for 5 days but not stable in ambient environment, the efficiency decreases 50% after standing in air for 30 hours (see Figure 10).

3. Conclusion

We report an inverted perovskite solar cell based on semi-transparent $CH_3NH_3PbBr_3$ film fabricated under the ambient atmosphere at moderate temperature (~ 100 ^oC). Inverted $CH_3NH_3PbBr_3$ cell using ICBA as an acceptor achieves a remarkably high Voc of 1.61 V which is the highest value among all reported perovskite solar cells. Solvent annealing of the active layer at room temperature has proved to be an effective way to improve the photovoltaic performance of the cell based on imperfect $CH_3NH_3PbBr_3$ film. The penetration of the acceptor molecules into perovskite to form a pseudo-bulk heterojunction structure and mend the defects of $CH_3NH_3PbBr_3$ film was evidenced by PL, TRPL spectra, SEM images and depth profile XPS data. The merit of using acceptor as a mending agent is no extra material is used, which can simplify the fabrication procedure and reduce the cost for mass production. Furthermore, ITO/PEDOT:PSS/$CH_3NH_3PbBr_3$/ICBA film is very transparent in the visible light. Low-temperature processed $CH_3NH_3PbBr_3$ solar cells with high Voc and semi-transparent absorber can be applied as the top cell for the

Nanoscale Accepted Manuscript

tandem solar cell.

4. Experimental section:

Materials and physicochemical studies.

Aqueous dispersion of PEDOT:PSS (1.3-.1.7 wt%, from H.C. Stark Baytron P AI 4083) was obtained from Heraeus Co. Fullerene derivatives ($PC_{71}BM$ (99.58%) and ICBA (99.5%)) were purchased from Solenne B. V., Netherlands. $PbBr_2$ (99.999%) was obtained from Aldrich. All the above materials were used as received. ITO-covered glass substrates purchased from Ruilong Co., Taiwan were photolithographically patterned in our laboratory with $HCl_{(aq)}$. CH_3NH_3Br (MABr) was synthesized as reported previously.[34] Uv/Vis absorption and PL spectra were recorded with Hitachi U-4100 spectrometers and F-7000 spectrometers, respectively. The thickness of the films was measured with a depth-profile meter (Veeco Dektak 150, USA). Five lines on the 1 cm × 1 cm film were made by carefully scratching with a tip and the average height between the hills and valleys was used to represent the film thickness. GIXRD data were collected in the 2θ range of 10-50 degrees on a Bruker powder diffractometer (D8 Discover) using Cu Kα1 radiation equipped with a 2D detector. Scanning Electron Micrograph (SEM) and Energy Dispersive Spectroscopy (EDS) were performed with a Hitachi S-800 microscopy at 15 KV. Samples (film on substrates) for SEM imaging and EDS study were mounted on a metal stub with a piece of conducting tape then coated with a thin layer of gold film to avoid charging. Time-resolved photoluminescence (TR-PL) spectra were conducted by the time-correlated single-photon counting (TCSPC) technique (UniRAM, Protrustech) along with the instrument response function of 200 ps and the excitation wavelength (repetition rate) was 405 nm (20 MHz).[40] To prevent laser-induced thermal effects, the diameter of the spot size on the sample was increased to 50 μm and the excitation power

Nanoscale Accepted Manuscript

was reduced to 0.1 mW. Depth profile X-ray photoelectron spectra were taken with a Perkin-Elmer PHI-590AM XPS/ESCA spectrometer system with a Cylindrical Mirror Electron (CMA) energy analyser. The X-ray sources were Al Kα at 600 W and Mg Kα at 400 W. XPS were taken at pass energy of 160 eV and 10 eV for survey scans and high-resolution scans, respectively. The sputtering time for each layer is 200 seconds.

Device fabrication and photovoltaic parameters measurements.

The procedure for fabricating the solar cells reported in this paper is very similar to that for preparing $CH_3NH_3PbI_3$ based devices we reported previously.[26] PEDOT:PSS was spin-coated on a heat pretreated patterned ITO under 5000 rpm for 50 sec and then annealed at 100 ^oC for 15 min. To deposit the perovskite layer, first a layer of $PbBr_2$ was spin-coated on top of PEDOT:PSS-coated ITO substrate from 0.5 M DMF solution using a spin rate of 2000 rpm for 30 seconds. And then CH_3NH_3Br (MABr) was spin-coated on top of $PbBr_2$ film from its isopropanol solution (with various concentrations, volumes and spin programs) to form $CH_3NH_3PbBr_3$ structure. Specifically, the highest efficiency device was fabricated with a concentration of CH_3NH_3Br/ isopropanol (IPA) *ca.* 15 mg/mL (30 μl) at a spin rate of 2000 rpm for 30 sec in a 1.5 cm x 1.5 cm substrate. After $CH_3NH_3PbBr_3$ film was formed, 24 wt% PCBM (or ICBA) in chlorobenzene was spin-coated onto the surface of perovskite layer at 1000 rpm, 30 sec to be an acceptor layer. All the fabrication procedures were carried out in an ambient atmosphere at room temperature. Solvent annealing of the active (donor/acceptor) layer was carried out by covering the PEDOT:PSS/ $CH_3NH_3PbBr_3$/PCBM (or ICBA) film with a petri dish for 24 hours in a glove box before the film was sent into the vacuum evaporator for depositing electrode. Finally PEDOT:PSS/$CH_3NH_3PbBr_3$/PCBM (or ICBA) film was transferred to a vacuum chamber to coat Ca/Al (20 nm/100 nm) electrode using thermal evaporation. The

Nanoscale Accepted Manuscript

device area is 0.5 cm × 0.2 cm. *I-V* curves of the cells were taken using a Keithley 4200 source measuring unit under a simulated AM1.5G sun light (Wacom solar simulator) at 100 $mWcm^{-2}$ and the light intensity was calibrated using a KG-5 Si diode. External quantum efficiency (EQE) or incident photo-to-current conversion efficiency (IPCE) was measured in air when the device was sealed with a Three-Bond sealer and measured right after taking out of glove box. A chopper and lock-in amplifier were used for the phase sensitive detection with a QE-R3011 measurement system (Enlitech Co., Taiwan). Cell for the stability test outside the glove box was fabricated using the same procedures except Ag, instead of Ca/Al, was used as an electrode.

Acknowledgements

Financial support from the Ministry of Science and Technology (MOST), Taiwan, ROC (grand number: NSC101-2113-M-008-008-MY3), is gratefully acknowledged. The devices fabrication and photovoltaic parameters measurements were carried out in Advanced Laboratory of Accommodation and Research for Organic Photovoltaics, MOST, Taiwan, ROC.

Supporting Information Available:

Supplementary data are collected in the electronic supporting information. The material is available online with the article.

Nanoscale Accepted Manuscript

REFERENCES

1 H. Snaith, J. *Phys. Chem. Lett.*, 2013, **4**, 3623-3630.

2 S. Kazim, M. K. Nazeeruddin, M. Grätzel and S. Ahmad, *Angew. Chem. Int. Ed.*, 2014, **53,** 2812-2824.

3 R F. Service, *Science* , 2014, **344,** 458-458.

4 N.-G. Park, *J. Phys. Chem. Lett.,* 2013, **4,** 2423–2429.

5 M. D. McGehee, *Nature*, 2013, **501**, 323-325.

6 H. Zhou, Q. Chen, G. Li, S. Luo, T. Song, S.-H. Duan, Z. Hong, J. You, Y. Liu and Y. Yang, *Science,* 2014, **345,** 542-546.

7 NREL (http://www.nrel.gov/ncpv/).

8 A. Kojima, K. Teshima, Y. Shirai and T. Miyasaka, *J. Am. Chem. Soc.,* 2009, **131**, 6050–6051.

9 E. Mosconi, A. Amat, M. K. Nazeeruddin, M. Grätzel and F. De Angelis, *J. Phys. Chem. C*, 2013, **117,** 13902-13913.

10 M. M. Lee, J. L. Teuscher, T. Miyasaka, T. N. Murakami and H. J. Snaith, *Science,* 2012, 338, 643-647.

11 J. You, Z. Hong, Y. Yang, Q. Chen, M. Cai, T.-B. Song, C.-C. Chen, S. Lu, Y. Liu, H. Zhou and Y. Yang, *ACS Nano*, 2014, **8,** 1674-1680.

12 L. Etgar, P. Gao, Z. Xue, Q. Peng, A. K. Chandiran, B. Liu, M. K. Nazeeruddin and M. Grätzel, *J. Am. Chem. Soc.,* 2012, **134,** 17396-17399.

13 G. E. Eperon, V. M. Burlakov, P. Docampo, A. Goriely and H. J. Snaith, *Adv. Funct. Mater.,* 2014, **24,** 151-157.

14 J. H. Noh, S. H. Im, J. H. Heo, T. N. Mandal and S. I. Seok, *Nano Lett.,* 2013, **13**, 1764-1769.

15 B. Cai, Y. Xing, Z. Yang, W.-H. Zhang and J. Qiu, *Energy Environ. Sci.,* 2013, **6,** 1480-1485.

Nanoscale Accepted Manuscript

16 E. Edri, S. Kirmayer, D. Cahen and G. Hodes, *J. Phys. Chem. Lett.,* 2013, **4,** 897-902.

17 S. Ryu, J. H. Noh, N. J. Jeon, Y. C. Kim, W. S. Yang, J. Seo and S. I. Seok, **Energy Environ. Sci.,** 2014, **7,** 2614-2618.

18 J. H. Heo, D. H. Song and S. H. Im, *Adv. Mater.,* 2014, **26,** 8179–8183.

19 E. Edri, S. Kirmayer, M. Kulbak, G. Hodes and D. Cahen, *J. Phys. Chem. Lett.,* 2014, **5**, 429-433.

20 T. Leijtens, G. E. Eperon, S. Pathak, A. Abate, M. M. Lee and H. J. Snaith, *Nat. Commun.,* 2013, **4,** 2885-2890.

21 J. Peet, A. J. Heeger and G. C. Bazan, *Acc. Chem. Res.,* 2009, **42,** 1700-1708.

22 W. Shockley and H. J. Queisser, *J. of Appl. Phys.,* 1961, **32**, 510-519.

23 P. Docampo, J. M. Ball, M. Darwich, G. E. Eperon and H. J. Snaith, *Nat Commun.,* 2013, **4,** 2761-2766.

24 A. Poglitsch and D. Weber, *J. Chem. Phys.,* 1987, **87**, 6373-6378.

25 T. B. Singh, N. Marjanovi´, G. J. Matt, S. G¨unes, N. S. Saricici, A. M. Ramil, A. Andreev, H. Sitter, R. Schw¨odiauer and S. Bauer, *Org. Electron.,* 2005, **6,** 105-110.

26 C.-H. Chiang, Z.-L. Tseng and C.-G. Wu, *J. Mater. Chem. A,* 2014, **2**, 15897-15903.

27 S. Aharon, B. E. Cohen and L. Etgar, *J. Phys. Chem. C,* 2014, **118**, 17160-17165.

28 S. Sun, T. Salim, N. Mathews, M. Duchamp, C. Boothroy, G. Xing, T. C. Sumbc, and Y. M. Lam, *Energy Environ. Sci.,* 2014, **7,** 399-407.

29 O. Malinkiewicz, A. Yella, Y. H. Lee, G. M. Espallargas, M. Graetzel, M. K. Nazeeruddin and H. J. Bolink, *Nat. Photo.,* 2014, **8**, 128-132.

30 J.-Y. Jeng, Y.-F. Chiang, M.-H. Lee, S.-R. Peng, T.-F. Guo, P. Chen and T.-C. Wen, *Adv. Mater.,* 2013, **25,** 3727–3732.

Nanoscale Accepted Manuscript

31 Y. He, H. Y. Chen, J. Hou and Y. Li, *J. Am. Chem. Soc.,* 2010, **132,** 1377-1382.

32 M. A. Green, K. Emery, Y. Hishikawa, W. Warta and E. D. Dunlop, *Prog. Photovolt: Res. Appl.,* 2015, **23**, 805-812.

33 M. I. Saidaminov1, A. L. Abdelhady, B. Murali, E. Alarousu, V. M. Burlakov, W. Peng, I. Dursun, L. Wang, Y. He, G. Maculan, A. Goriely, T. Wu, O. F. Mohammed, O.M. Bakr, *Nat. Commun.* DOI: 10.1038/ncomms8586.

34 B. J. Skromme, C. J. Sandroff, E. Yablonovitch and T. Gmitter, *Appl. Phys. Lett.,* 1987, **51**, 2022–2024.

35 A. Abate, M. Saliba, D. J. Hollman, S. D. Stranks, K. Wojciechowski, R. Avolio and H. J. Snaith, *Nano Lett.,* 2014, **14,** 3247-3254.

36 N. K. Noel, A. Abate, S. D. Stranks, E. S. Parrott, V. M. Burlakov, A. Goriely and H. J. Snaith, *ACS Nano,* 2014, **8,** 9815–9821.

37 J. Zhang, Z. Hu, L. Huang, G. Yue, J. Liu, X. Lu, Z. Hu, M. Shang, L. Han and Y. Zhu, *Chem. Commun.,* 2015, **51,** 7047-7050.

38 S. H. Chang. K.-F. Lin, H.-M. C.-C. Chen, W.-T. Wu, W.-N. Chen, P.-J. Wu, S.-H. Chen and C.-G. Wu, Sol. Energy Mat. Sol. Cell, 2016, **145**, 375-381.

39 S. H. Chang, C.-H. Chiang, H.-M. Cheng, C.-Y. Tai and C.-G. Wu, Opt. Lett., 2013, **38**, 5342-5345.

40 S. H. Chang, C.-H. Chiang, Z.-L. Tseng, K.-Y. Chiu, C.-Y. Tai and C.-G. Wu, J. Phys. D: Appl. Phys., 2015, **48**, 195104.

41 H. J. Snaith, A. Abate, J. M. Ball, G. E. Eperon, T. Leijtens, N. K. Noel, S. D. Stranks, J. T.-W. Wang, K. Wojciechowski and W. Zhang, *J. Phys. Chem. Lett.,* 2014, **5**, 1511-1515.

42 M. R. Filip, G. E. Eperon, H. J. Snaith and F. Giustino, *Nat. Commun.,* 2014, **5**, 5757-5760.

Nanoscale Accepted Manuscript

Figure captions:

Figure 1: The process for the fabrication of the inverted $CH_3NH_3PbBr_3$ solar cell. (S.C.: Spin Coating; T.E.: Thermal Evaporation)

Figure 2: SEM images of $PbBr_2$ film, $MAPbBr_3$ films fabricated with one-step and two-step methods.

Figure 3: XRD patterns of $MAPbBr_3$ films prepared with various concentrations of MABr/IPA solutions.

Figure 4: Energy level diagram of the components for the inverted perovskite solar cells.

Figure 5: (a) The IPCE curve of the champion cell. (b) Uv/Vis absorption spectrum of the corresponding $MAPbBr_3$ film.

Figure 6: Penetration of ICBA molecules into the voids/grain boundaries of $MAPbBr_3$ film upon solvent annealing.

Figure 7: (a) PL spectra of $CH_3NH_3PbBr_3$ (Psk) film, Psk/PCBM and Psk/ ICBA films with and without solvent annealing (SA). (b) TRPL spectra of $CH_3NH_3PbBr_3$ (Psk) and Psk/ ICBA films with and without solvent annealing.

Figure 8: Cross section SEM images of ITO/PEDOT:PSS/$CH_3NH_3PbBr_3$/ICBA films with and without solvent annealing.

Figure 9: Depth profile XPS analysis of oxygen content.

Figure 10: Long-term stability of the champion inverted $MAPbBr_3$ solar cell stored in glove box and exposed in air.

Nanoscale Accepted Manuscript

Table 1. Photovoltaic parameters for the inverted solar cell based on $CH_3NH_3PbBr_3$ film fabricated with various concentrations (conc.) of MABr/IPA solutions and using different acceptors.

[1]MABr/IPA conc. (mg/mL)	Acceptor	Solvent annealing	Jsc (mA/cm^2)	Voc (mV)	*FF*	η (%)
15	PCBM	No	1.94	1.38	0.32	0.86
15	PCBM	Yes	5.20	1.38	0.78	5.60
10	PCBM	Yes	3.25	1.00	0.46	1.50
20	PCBM	Yes	4.78	1.36	0.58	3.77
15	ICBA	No	2.49	1.60	0.43	1.71
15	ICBA	Yes	6.04	[2]1.61	0.77	7.50

1. The volume of MABr/IPA solution is 30 μL
2. The Voc statistics (based on 29 devices) of the cell are displayed in Figure S6, ESI.

Nanoscale Accepted Manuscript

Figure 1:

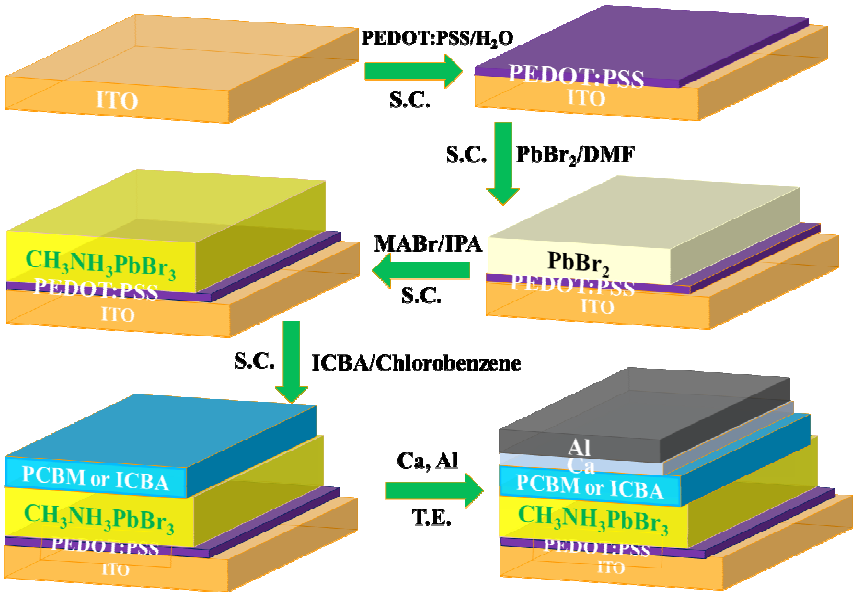

Nanoscale Accepted Manuscript

Figure 2

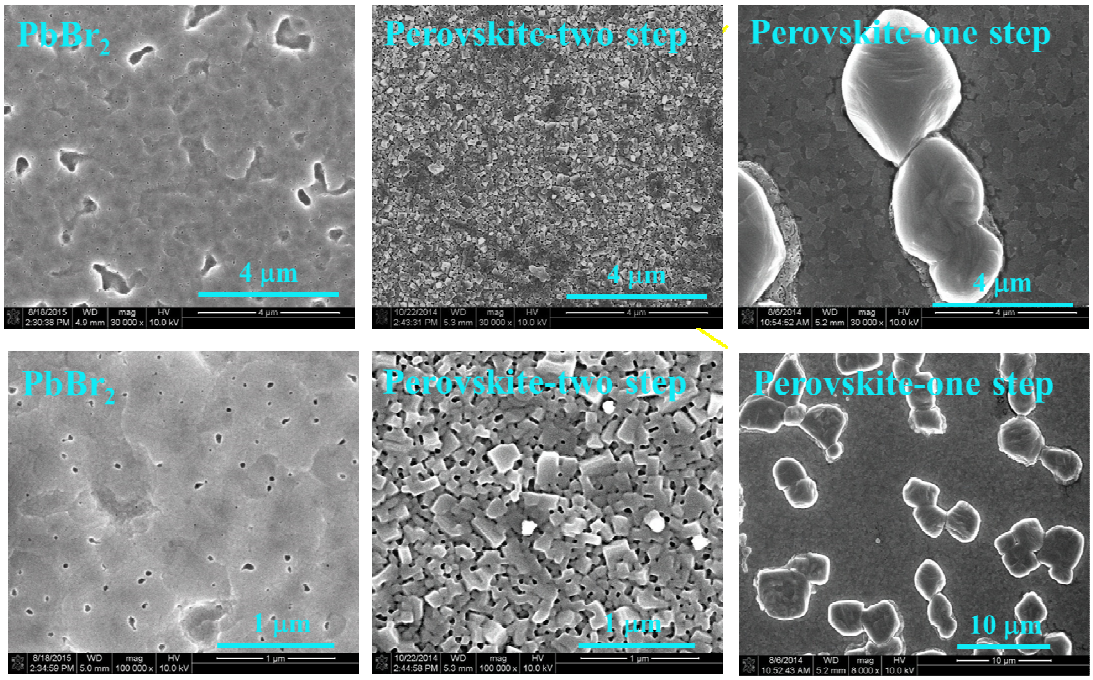

Nanoscale Accepted Manuscript

Figure 3

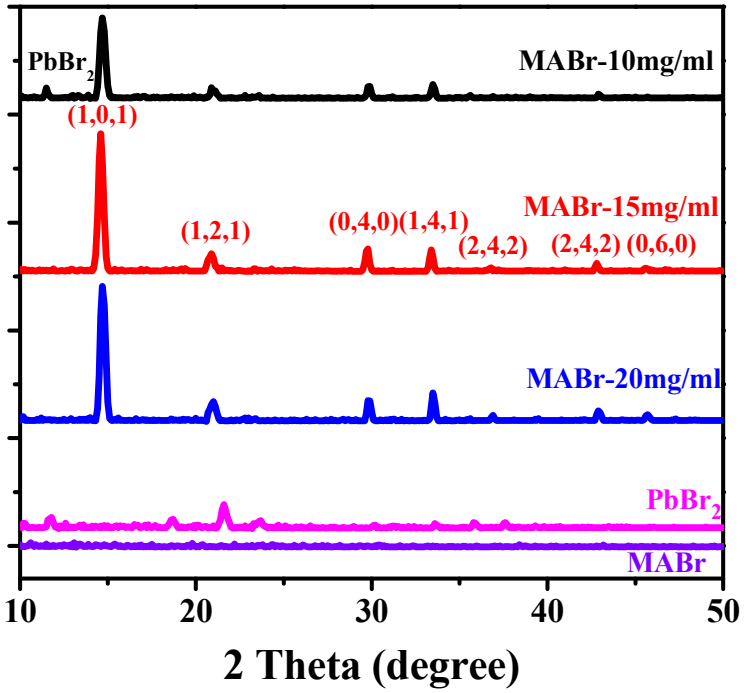

Nanoscale Accepted Manuscript

Figure 4.

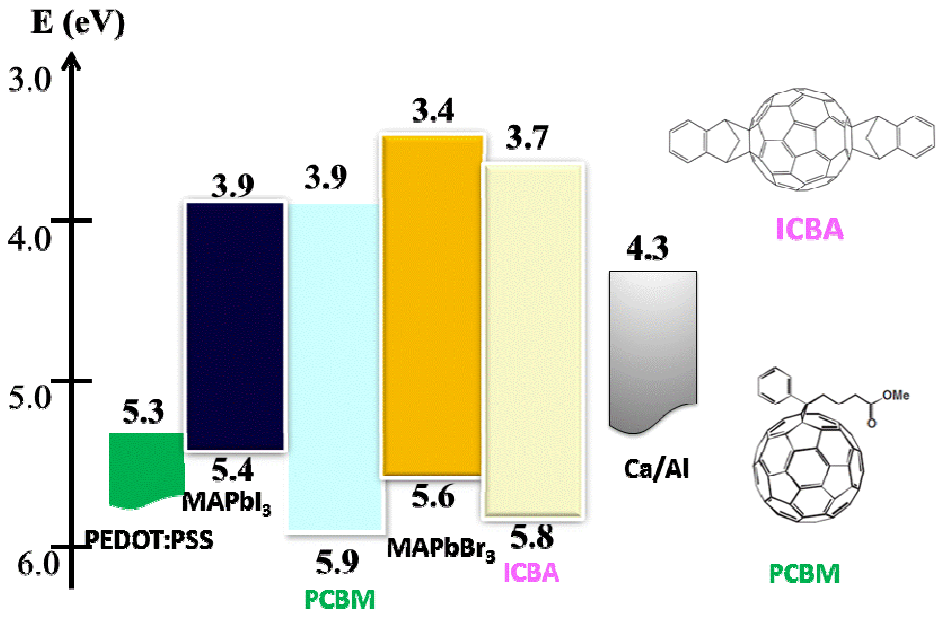

Nanoscale Accepted Manuscript

Figure 5.

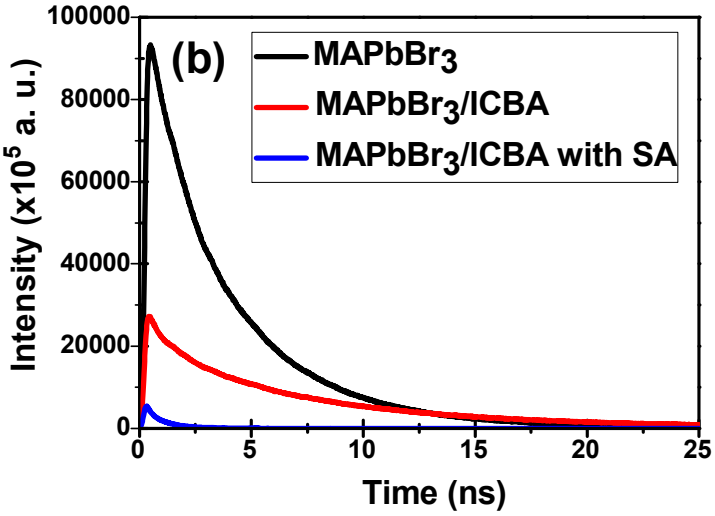

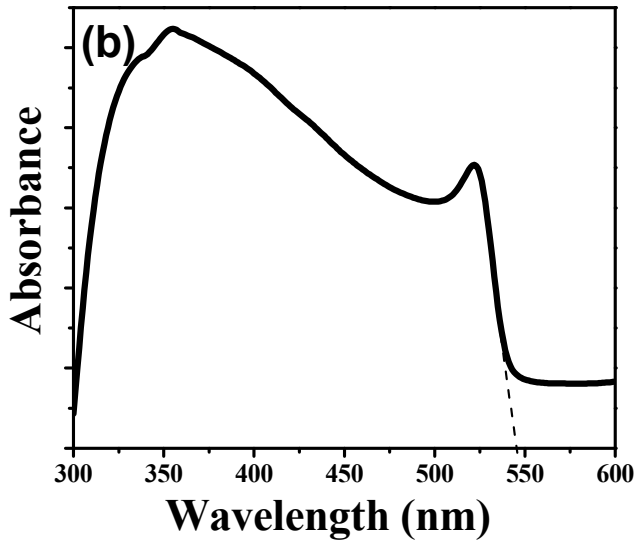

Nanoscale Accepted Manuscript

Figure 6

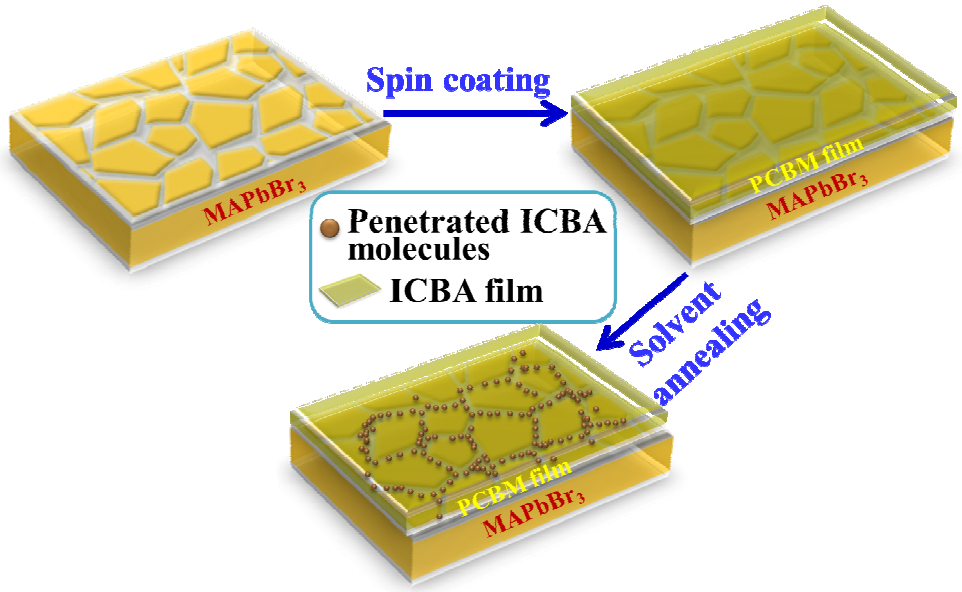

Nanoscale Accepted Manuscript

Figure 7

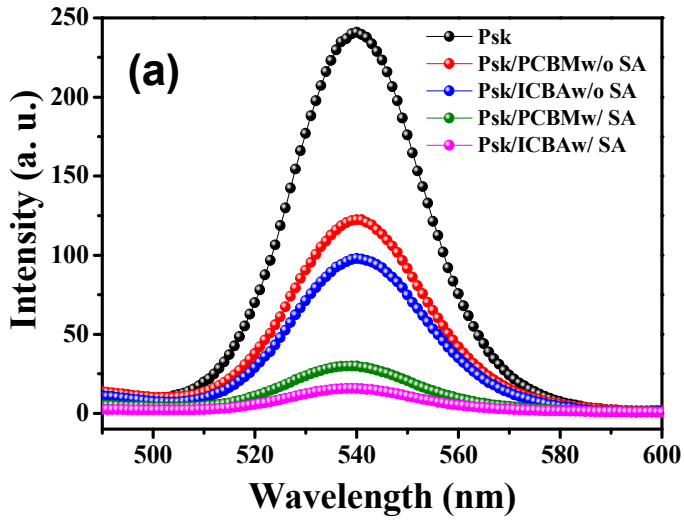

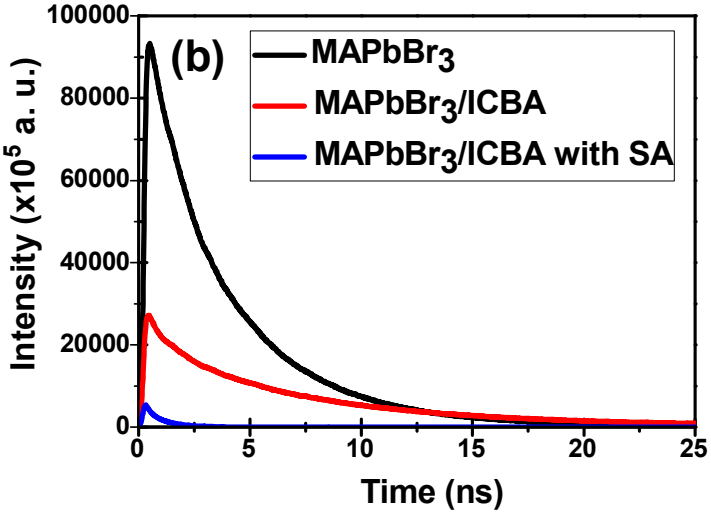

Nanoscale Accepted Manuscript

Figure 8.

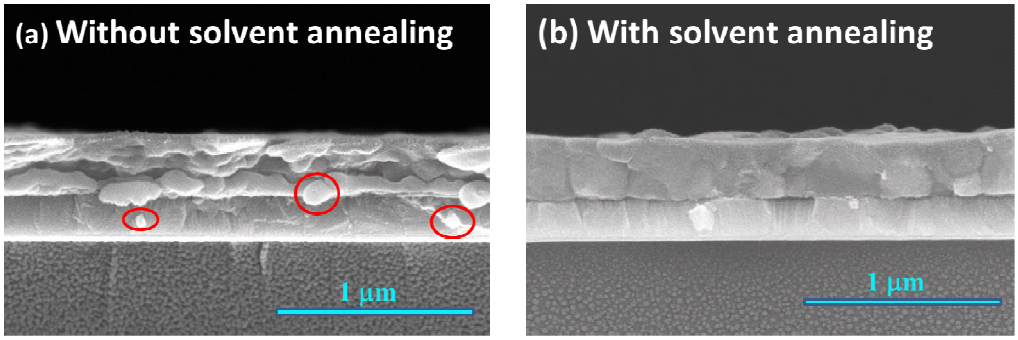

Nanoscale Accepted Manuscript

Figure 9.

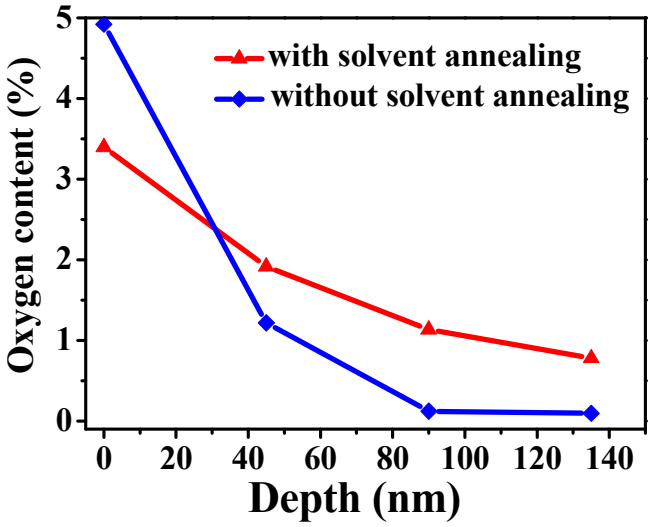

Nanoscale Accepted Manuscript

Figure 10

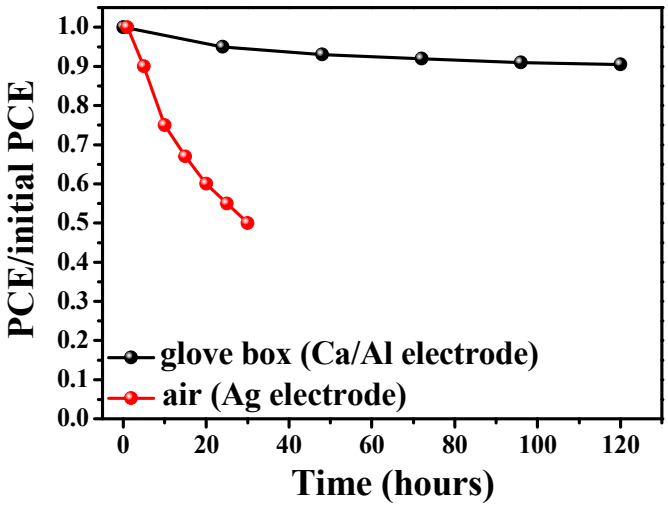

Nanoscale Accepted Manuscript